

LETTER TO THE EDITOR

GMRT radio observations of the transiting extrasolar planet HD189733 b at 244 and 614 MHz^{*}

A. Lecavelier des Etangs^{1,2}, S. K. Sirothia³, Gopal-Krishna³, and P. Zarka⁴

¹ CNRS, UMR 7095, Institut d'Astrophysique de Paris, 98^{bis} boulevard Arago, F-75014 Paris, France

² UPMC Univ. Paris 6, UMR 7095, Institut d'Astrophysique de Paris, 98^{bis} boulevard Arago, F-75014 Paris, France

³ National Centre for Radio Astrophysics, TIFR, Post Bag 3, Pune University Campus, Pune 411007, India

⁴ LESIA, Observatoire de Paris, CNRS, UPMC, Université Paris Diderot, 5 Place Jules Janssen, 92190 Meudon, France

ABSTRACT

We report a sensitive search for meter-wavelength emission at 244 and 614 MHz from HD189733 b, the nearest known extrasolar transiting planet of ‘hot-Jupiter’ type. To discriminate any planetary emission from possible stellar or background contributions, we observed the system for 7.7 hours encompassing the planet’s eclipse behind the host star. These GMRT observations provide very low (3σ) upper limits of 2 mJy at 244 MHz and 160 μ Jy at 614 MHz. These limits are, respectively, about 40 and 500 times deeper than those reported recently at a nearby frequency of 340 MHz. Possible explanations of our non-detection include: (1) the Earth being outside the planet’s emission beam; (2) its highly variable emission with more rapid flaring than the temporal sampling in our observations; (3) the planetary emission being intrinsically too weak; or more likely, (4) the emission being predominantly at lower frequencies because of a weak planetary magnetic field. We briefly discuss these possibilities and the constraints on this exo-planetary system environment.

Key words. Stars: planetary systems - Stars: individual: HD189733 - Stars: coronae - Techniques: interferometric

1. Introduction

The detection of radio emission from an extrasolar planet would be a major step in the characterization of these planets and their environment, possibly providing information about the planetary magnetic field and the interaction of the planet with the stellar magnetic field and corona. In parallel with theoretical estimates for radio emission from a large number of extrasolar planets (*e.g.*, Grießmeier et al. 2007), searches for decameter- and meter-wavelength radio emission from a few extrasolar planets have been undertaken (*e.g.*, Bastian et al. 2000; Ryabov et al. 2004; Winterhalter et al. 2005; George & Stevens 2007; Lazio & Farrell 2007). Radio detections seem currently feasible only provided that the planets are 10^3 to 10^4 times stronger emitters than Jupiter. However, the extreme conditions of ‘hot-Jupiters’ could make this happen because of the extreme incident Poynting flux (Zarka 2007), justifying the radio-magnetic scaling law proposed in Zarka et al. (2001). At any rate, all the estimates of cyclotron maser decametric emission involve several unknowns, *e.g.*, stellar winds, coronal density, and stellar and planetary magnetic fields.

So far only non-detections have been reported, the telescopes used being UTR (10-30 MHz, $\sigma \sim 1.6$ Jy), VLA (74 MHz, $\sigma \sim 50$ mJy), and GMRT (150 MHz, $\sigma \sim 10$ mJy; see review in Lazio et al. 2009). The principal contributors to the noise level at these low frequencies are the sky background, radio frequency interference, and iono-

spheric scintillations, which distort the incoming signal and increase the noise. Hence, interferometric observations of high sensitivity and resolution hold considerable promise for improvement. In particular, the Giant Metrewave Radio Telescope (GMRT), a 30-km baseline array consisting of 30 dishes of 45 metre diameter each (Swarup 1990), appears to be the telescope of choice. We report the first GMRT search targeted at the planet HD189733 b, which is one of the best candidates among the known ‘hot-Jupiter’ extrasolar planets (Sect. 2). Our search is over an order-of-magnitude deeper than the recently reported search for meter-wavelength emission from this system based on single-dish observations at 307-347 MHz (Smith et al. 2009).

2. The target planet: HD 189733 b

Located just 19.3 parsecs away, HD189733 b is one of the most prominent extrasolar planets known (Bouchy et al. 2005). With a semi-major axis of 0.03 AU and an orbital period of 2.2 days, it belongs to the class of ‘very hot-Jupiters’. More importantly, since this planet is seen to transit its parent star, the planetary transits and eclipses can be used to probe the planet’s atmosphere and environment (*e.g.*, Charbonneau et al. 2008, Désert et al. 2009).

HD189733b orbits a small and bright main-sequence K-type star, and shows a transit occultation depth of $\approx 2.5\%$ at optical wavelengths (Pont et al. 2007). The planet has a mass $M_p = 1.13$ Jupiter masses (M_{Jup}) and a radius $R_p = 1.16$ Jupiter radii (R_{Jup}) in the visible (Bakos et al. 2006; Winn et al. 2007). The short period of the planet (2.21858 days) has been measured precisely (Hébrard & Lecavelier des Etangs 2006; Knutson et al.

^{*} Data for this observations can be retrieved electronically on the GMRT archive server <http://ncra.tifr.res.in/~gmrtarchive> and by request to archive@gmrt.ncra.tifr.res.in.

2009). Spectropolarimetry has measured the strength and topology of the stellar magnetic field, which reaches up to 40 G (Moutou et al. 2007). Sodium has been detected in the planet’s atmosphere by ground-based observations (Redfield et al. 2008). Using the ‘Advanced Camera for Survey’ aboard the Hubble Space Telescope (HST), Pont et al. (2008) detected atmospheric haze, which is interpreted as Mie scattering by small particles (Lecavelier des Etangs et al. 2008). CO molecules have been tentatively proposed to explain the excess absorption seen at $4.5 \mu\text{m}$ (Charbonneau et al. 2008; Désert et al. 2009). Absorption in Lyman- α observed with the HST/ACS is explained in terms of atomic hydrogen escaping from the planet’s exosphere at a rate of 10^7 - 10^{11} g/s (Lecavelier des Etangs et al., in preparation).

The atmosphere and environment of transiting planets can also be studied using the planetary eclipse techniques. The principle is to subtract the signal received when the planet is hidden behind the star, from observations made before and after this eclipse. This allows reliable extraction of the planetary emission. This technique has enabled detection of thermal infrared emission from the extrasolar planets HD 209458 b and TReS-1 (Charbonneau et al. 2005; Deming et al. 2005). Using Spitzer spectroscopy of planetary eclipses, the infrared spectra of HD189733 b atmosphere have revealed signatures of H_2O absorption and possibly weather-like variations in the atmospheric conditions (Grillmair et al. 2009).

We have developed a similar strategy by monitoring the radio flux from the HD 189733 b system before, during, and after a planetary eclipse. By comparing the radio flux levels, we can thus discriminate between any radio emission contributed by the planet and the star (or any other background source within the synthesized beam).

3. Observations and data analysis

Using GMRT, we performed simultaneous dual-frequency observations of the HD189733 b field at 244 MHz and 614 MHz on 2008 August 14. The phase centre was set at the star’s position of $\alpha_0=20\text{h}00\text{m}43.7\text{s}$, $\delta_0=+22^\circ42'39''$ (J2000). The observations started at 13h50m and finished at 22h20m (UT), covering the full passage of the target in the visibility window of the sky and the planet’s eclipse behind the star, which took place between 15h55m and 17h43m (UT). At 244 MHz, the receiver bandwidth was 5.6 MHz (LL polarization only) and at 614 MHz the bandwidth was 32 MHz (RR polarization only). At each frequency, the visibility integration time was 16.78 seconds and the total observation time was 7.71 hours, on both the primary field and the calibration sources. Because of a temporary system failure, roughly in the middle of the run, most of the antennas could not be used for ~ 1.5 hours from 16h36m to 18h10m (UT). Although this observing ‘gap’ substantially overlapped with the planet’s occultation behind the star, this problem should not affect our main conclusions.

At both frequencies, 3C48 was observed as the primary flux density and bandpass calibrator, for a total of 0.27 hours. The source 2052+365 was chosen as a phase calibrator and observed repeatedly for a total of 0.8 hours. The total acquisition time on the target field was 6.45 hours.

The data reduction was completed mainly using the AIPS++ package (version: 1.9, build #1556). After apply-

ing bandpass corrections using 3C48, gain and phase variations were quantified and used for the flux density, bandpass, gain, and phase calibration of the target field data; for 3C48, we assumed flux densities of 51.16 Jy and 29.305 Jy at 244 MHz and 614 MHz, respectively.

While calibrating the data, bad data points were flagged at various stages. The data for antennas with relatively large errors in antenna-based gain solutions were examined and flagged over certain time ranges. Some baselines were flagged, based on closure errors on the bandpass calibrator. Channel and time-based flagging of the data points corrupted by radio frequency interference (RFI) was done by applying a median filter with a 6σ threshold. Residual errors above 5σ were also flagged after a few rounds of imaging and self-calibration. The system temperature (T_{sys}) was found to vary among the antennas, and also with the ambient temperature and elevation (Sirothia 2009). In the absence of regular T_{sys} measurements for GMRT antennas, this correction was estimated from the residuals of calibrated data with respect to the model data. The corrections were then applied to the data. The final image was made after several rounds of phase self-calibration, and one round of amplitude self-calibration, where the data were normalized by the median gain found for the entire data. The final image was also corrected for the primary beam shape taken to be a Gaussian with FWHM of $117.0'$ and $42.7'$ at the reference frequencies of 235 MHz and 610 MHz, respectively. The final images have median RMS noises of about 470 and $39 \mu\text{Jy}$ per beam, at 244 MHz and 614 MHz, respectively. For the central $5' \times 5'$ region shown in Fig. 1, we have $\sigma=685 \mu\text{Jy}$ at 244 MHz and $\sigma=53 \mu\text{Jy}$ at 614 MHz.

After the final imaging stage, light curves were generated for a synthesized-beam size region centered on the coordinates of the star and two randomly chosen control directions a few arc minutes offset from the star. To obtain these light curves, we calculated model visibilities using the sources detected in the entire field-of-view excluding a synthesized beam-wide region centered on the desired location (α_0, δ_0); we then subtracted this model out from the final calibrated visibility data. The residual visibility data (RVD) were then phase-centered on α_0, δ_0 and averaged for desired time bins to generate the light curves. Figure 2 shows the resulting light curve for the star’s position.

4. Results and discussion

4.1. Results

For the stellar+planetary emission, the GMRT images (Fig. 1) provide 3σ upper limits of 2 mJy at 244 MHz and $160 \mu\text{Jy}$ at 610 MHz. We note that the 244 MHz map shows a chain of peaks roughly along position angle $PA \sim 35^\circ$, but offset eastward from the star’s position by about four beam widths. These peaks appear to be artefacts from the residual phase errors dominated by the bright extended planetary nebula M27 in the field-of-view. The upper limit of 2 mJy (3σ for the $5' \times 5'$ field) is 2σ for the $1' \times 5'$ rectangular strip oriented at $PA \sim 35^\circ$ that encompasses the chain of artifacts ($\sigma=1.05 \text{ mJy}$).

Using the light curve, we also searched for a planet’s emission eclipse or flares. With average flux densities before, during, and after the secondary transit of $1.8 \pm 0.8 \text{ mJy}$, $2.7 \pm 1.7 \text{ mJy}$, and $-0.4 \pm 0.6 \text{ mJy}$ at 244 MHz, and $-0.16 \pm 0.09 \text{ mJy}$, $-0.38 \pm 0.15 \text{ mJy}$, and $0.07 \pm 0.07 \text{ mJy}$ at

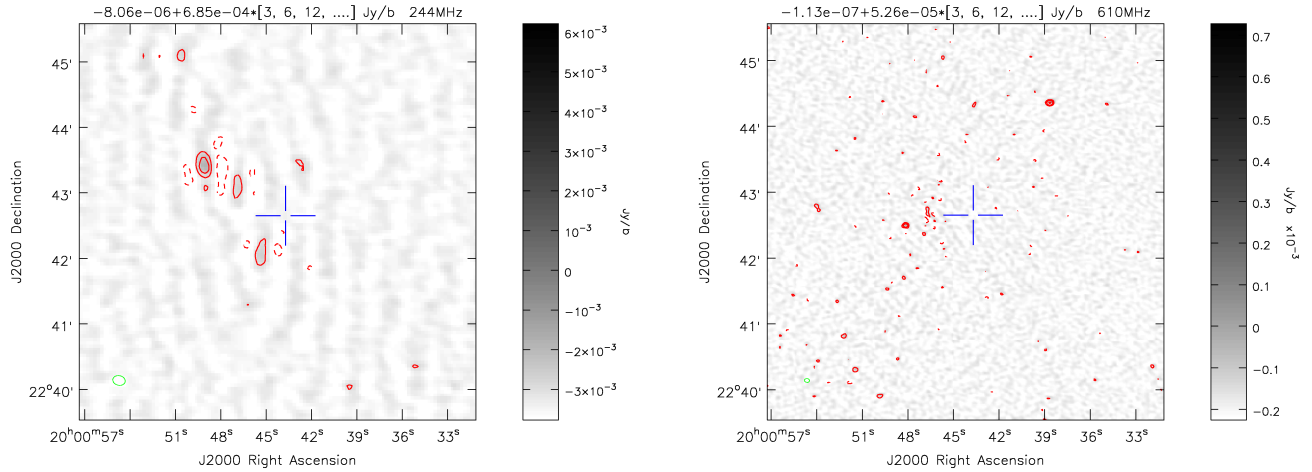


Fig. 1. GMRT image of HD189733 field at 244 MHz (left panel) and 614 MHz (right panel). The ellipse in the lower left corner of each image shows the half power beamwidth ($11.54'' \times 8.82''$, $77^\circ.6$ at 244 MHz and $4.76'' \times 3.45''$, $82^\circ.5$ at 614 MHz). The contour levels given at the top of the images are in units of Jy beam^{-1} and are defined as $\text{mean} + \text{rms} \times (n)$ where n is an integer. Negative contours appear as dashed lines.

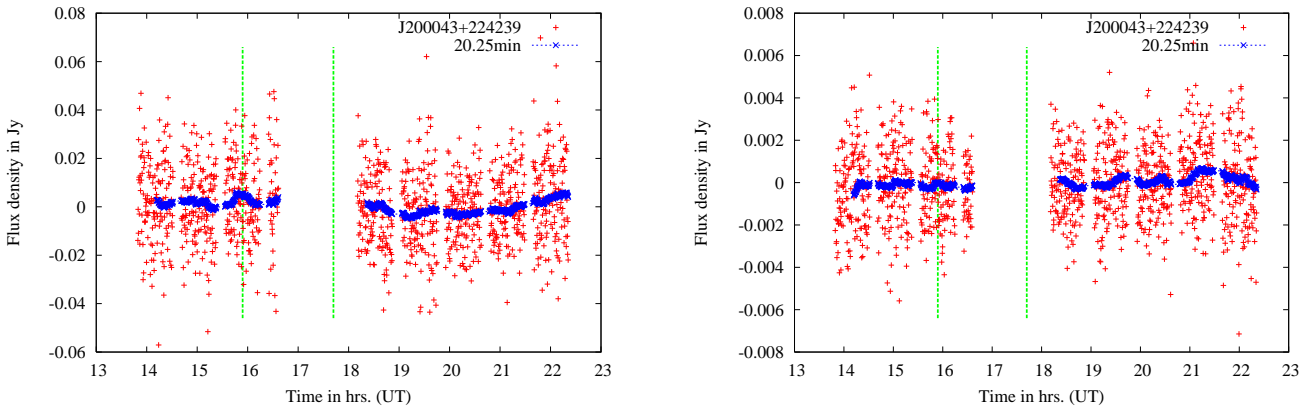


Fig. 2. Time series of the flux density measured at 244 MHz (left panel) and 614 MHz (right panel) in the direction of HD189733 (red crosses), for a time sampling of 16.78 sec. The vertical dotted green lines indicate the beginning and the end of the planet's eclipse behind the star. The thick (blue) curves show the flux densities averaged in 20.25 minute bins.

614 MHz, respectively, we did not detect an eclipse signature. Using the running averages of the light curve, obtained for intervals between 1 and 30 minutes, no emission flare events were found at either frequency (Fig. 2). We therefore conclude a non-detection of planetary radio emission. We note that the planet's eclipse times plotted in Fig. 2 (green lines) are calculated using the size of the planet in the optical. If radio emission originates in a region larger than the planet, the ingress could happen earlier and the egress later. However, emission at frequencies above 200 MHz is expected to originate in the very inner regions of the planet magnetosphere, and the eclipse times are expected to be similar to that of the planet itself.

Theoretical and observational aspects of the radio emission from extrasolar planets are discussed *e.g.*, in Zarka (2007), where the generalized concept of flow-obstacle interaction is developed. Accordingly, the present non-detection of HD189733 b may occur because : (1) the Earth was outside the planet's emission beam, at least at the time

of observation, or (2) the emission is highly variable with flares much faster than the temporal sampling of our observations, or (3) the planetary emission was simply too weak intrinsically, or, perhaps more likely (4) the planetary emission peaks at frequencies much lower than 200 MHz, because of a weak planetary magnetic field.

4.2. Emission beam

Cyclotron maser emission is rather confined within a beam solid angle. It is therefore possible that even strong emission remains unobservable from the Earth. For instance, if we assume that the magnetic axis is not too misaligned with the rotation axis and that emission is produced at the highest cyclotron frequencies (*i.e.*, very near the planetary poles), then the typical beaming angle of $\sim 50^\circ$ - 60° may account for the non-detection. However, in case of a magnetic axis tilted with respect to the rotation axis the geometric explanation of the non-detection becomes less plausible.

This issue can be clarified by observing the same target at multiple epochs.

4.3. Flaring emission

If the emission is sporadic, it may have been missed because of our time sampling of 16 s. However, this is not the most likely explanation because even in the case of Jupiter's flares, the duty cycle within the time-frequency space is between 15 and 30%. The corresponding dilution factor is only between 3 and 6, and is not crucial given the large uncertainties in the other parameters of the system.

4.4. Emission flux

For the three mechanisms considered: i.e., kinetic emission, magnetic emission, and coronal mass ejection, the corresponding radio flux density estimates should reach 0.4, 900, and 30 mJy, respectively (Greissmeier 2007). The magnetic emission is the favored alternative but the emission is expected to peak at just a few MHz, i.e., at frequencies much lower than those covered in the present observations.

Nonetheless, there is another possible scenario. For an intense magnetic field (of up to 40 G; Moutou et al. 2007), an active chromosphere (Boisse et al. 2009), and a rapid rotation (11.7 days period; Hébrard & Lecavelier des Etangs 2006; Croll et al. 2007), the stellar magnetosphere can extend beyond the orbit of the extrasolar planet whose semi-major axis is only 0.03 AU (see discussion in Jardine & Cameron 2008). Assuming that the emission is produced by an interaction between the planetary magnetosphere and the stellar corona in which it is embedded, and using Eq. 17 and the numerical values from the model of Jardine & Cameron (2008), with a 10% efficiency of conversion of the power of accelerated electrons into radio emission and an emission beam solid angle of 1.6 sr, the predicted radio flux from HD189733 b is about 15 mJy. With this model and assuming that our non-detection of emission from HD189733 b is caused by its low intrinsic intensity, the upper limits of 2 mJy at 244 MHz and 0.16 mJy at 614 MHz can be translated into upper limits for the stellar coronal density of 0.36 and 0.1 times the solar coronal density, respectively.

4.5. Emission frequency

The principal mechanism advocated for radio emission is the electron-cyclotron maser radiation. It occurs at the local gyrofrequency f_g given by, $f_g = 2.8 (B_p/1 \text{ G}) \text{ MHz}$, where B_p is the planet's magnetic field strength. The non-detection could then be attributed to a weak planetary magnetic field, such that the gyrofrequency falls below our observation frequencies. The observed frequencies of 244 and 614 MHz would then correspond to planetary magnetic fields of 85 G and 220 G, respectively. We recall that the Jovian magnetic field strength estimated from the radio frequency cut-off of its cyclotron emission is around 40 G.

Finally, cyclotron maser emission can also be quenched by a too high plasma frequency (f_{pe}) in the source region (Zarka 2007). With a 40 G magnetic field, the condition for quenching (f_{pe} larger than a tenth of the cyclotron frequency) implies an electron density larger than about

$1.5 \times 10^6 \text{ cm}^{-3}$ in the low stellar corona, a condition which is not implausible.

5. Conclusion

In summary, our radio observations of HD189733 b have provided very tight upper limits at 244 MHz and 614 MHz, which are below some predictions reported in the literature. The non-detection could be attributed to the inadequate time sampling rate of the observation, beam focusing, or intrinsic emission power being lower than theoretical predictions. The frequencies of our observations would require strong planetary magnetic field, and so we favor the scenario of a low magnetic field as an explanation of our non-detection. Better prospects are clearly offered by observations at lower frequencies, which will become feasible with UTR2, LOFAR (planned in short-term future), and SKA (long-term future).

Acknowledgements. We thank the anonymous referee for the helpful comments. We thank the staff of the GMRT who have made these observations possible. Special thanks are due to J. P. Kodilkar for his help in executing the observations. GMRT is run by the National Centre for Radio Astrophysics (NCRA) of the Tata Institute of Fundamental Research (TIFR). P.Z. activities in radio search for exoplanets are partly supported by ANR program NT05-1_42530 "Radio-Exopla".

References

- Bakos, G. Á., Knutson, H., Pont, F., et al. 2006, *ApJ*, 650, 1160
 Bastian, T. S., Dulk, G. A., & Leblanc, Y. 2000, *ApJ*, 545, 1058
 Boisse, I., Moutou, C., Vidal-Madjar, A., et al. 2009, *A&A*, 495, 959
 Bouchy, F., Udry, S., Mayor, M., et al. 2005, *A&A*, 444, L15
 Charbonneau, D., Allen, L. E., Megeath, S. T., et al. 2005, *ApJ*, 626, 523
 Charbonneau, D., Knutson, H. A., Barman, T., et al. 2008, *ApJ*, 686, 1341
 Croll, B., Matthews, J. M., Rowe, J. F., et al. 2007, *ApJ*, 671, 2129
 Deming, D., Seager, S., Richardson, L. J., & Harrington, J. 2005, *Nature*, 434, 740
 Deming, D., Harrington, J., Seager, S., & Richardson, L. J. 2006, *ApJ*, 644, 560
 Desert, J.-M., Lecavelier des Etangs, A., Hébrard, G., et al. 2009, arXiv:0903.3405
 George, S. J., & Stevens, I. R. 2007, *MNRAS*, 382, 455
 Griessmeier, J.-M., Zarka, P., Spreuw, H. 2007 *A&A*, 475, 359
 Grillmair, C. J., Burrows, A., Charbonneau, D., et al. 2009, *Nature*, 456, 767
 Hébrard, G., & Lecavelier Des Etangs, A. 2006, *A&A*, 445, 341
 Jardine, M., & Cameron, A. C. 2008, *A&A*, 490, 843
 Knutson, H. A., Charbonneau, D., Cowan, N. B., et al. 2009, *ApJ*, 690, 822
 Lecavelier Des Etangs, A., Pont, F., Vidal-Madjar, A., & Sing, D. 2008, *A&A*, 481, L83
 Lazio, T. J. W., & Farrell, W. M. 2007, *ApJ*, 668, 1182
 Pont, F., Gilliland, R. L., Bryden, G., et al. 2009, arXiv:0903.0873
 Lecavelier des Etangs, A., Pont, F., Vidal-Madjar, A., & Sing, D. 2008, *A&A*, 481, L83
 Moutou, C., Donati, J.-F., Savalle, R., et al. 2007, *A&A*, 473, 651
 Pont, F., Gilliland, R. L., Moutou, C., et al. 2007, *A&A*, 476, 1347
 Pont, F., Knutson, H., Gilliland, R. L., Moutou, C., & Charbonneau, D. 2008, *MNRAS*, 385, 109
 Redfield, S., Endl, M., Cochran, W. D., & Koesterke, L. 2008, *ApJ*, 673, L87
 Ryabov, V. B., Zarka, P., & Ryabov, B. P. 2004, *Planet. Space Sci.*, 52, 1479
 Sirothia S. K. 2009, *MNRAS* submitted
 Smith, A. M. S., Cameron, A. C., Greaves, J., et al. 2009, *MNRAS*, 395, 335
 Swarup, G. 1990, *Indian Journal of Radio and Space Physics*, 19, 493
 Winn, J. N., Holman, M. J., Henry, G. W., et al. 2007, *AJ*, 133, 1828

- Winterhalter, D., Majid, W., Kuiper, T., et al. 2005, Bulletin of the American Astronomical Society, 37, 1292
- Zarka, P. 2007, Planet. Space Sci., 55, 598
- Zarka, P., Treumann, R. A., Ryabov, B. P., & Ryabov, V. B. 2001, Ap&SS, 277, 293